Received: 12 December 2019 | Revised: 24 June 2020 | Accepted: 5 July 2020

DOI: 10.1111/bph.15195

RESEARCH PAPER

# Antidiabetic activity in vitro and in vivo of BDB, a selective inhibitor of protein tyrosine phosphatase 1B, from *Rhodomela confervoides*

Jiao Luo[2,3] | Meiling Zheng[6] | Bo Jiang[3,5] | Chao Li[3,5] | Shuju Guo[3,5] | Lijun Wang[3,5] | Xiangqian Li[1,4] | Rilei Yu[6] | Dayong Shi[1,4]

[1]State Key Laboratory of Microbial Technology, Shandong University, Jinan, China

[2]School of Public Health, Qingdao University, Qingdao, China

[3]CAS Key Laboratory of Experimental Marine Biology, Institute of Oceanology, Chinese Academy of Sciences, Qingdao, China

[4]Laboratory for Marine Biology and Biotechnology, Qingdao National Laboratory for Marine Science and Technology, Qingdao, China

[5]Center for Ocean Mega-Science, Chinese Academy of Sciences, Qingdao, China

[6]Key Laboratory of Marine Drugs, Chinese Ministry of Education, School of Medicine and Pharmacy, Ocean University of China, Qingdao, China

**Correspondence**
Jiao Luo, School of Public Health, Qingdao University, Qingdao 266071, China.
Email: luojiao2012@163.com

Dayong Shi, State Key Laboratory of Microbial Technology, Shandong University, Jinan 250100, China.
Email: shidayong@sdu.edu.cn

**Funding information**
Qingdao Marine Biomedical Science and Technology Innovation Center project, Grant/Award Numbers: 2017-CXZX01-1-1, 2017-CXZX01-3-9; NSFC-Shandong Joint Fund, Grant/Award Number: U1706213; Shandong Provincial Natural Science Foundation for Distinguished Young Scholars, Grant/Award Number: JQ201722; Fund of Taishan scholar project; National Program for Support of Top-notch Young Professionals; Key Research Program of Frontier Sciences,

**Background and Purpose:** Protein tyrosine phosphatase (PTP) 1B (PTP1B) plays a critical role in the regulation of obesity, Type 2 diabetes mellitus and other metabolic diseases. However, drug candidates exhibiting PTP1B selectivity and oral bioavailability are currently lacking. Here, the enzyme inhibitory characteristics and pharmacological benefits of 3-bromo-4,5-bis(2,3-dibromo-4,5-dihydroxybenzyl)-1,2-benzenediol (BDB) were investigated in vitro and in vivo.

**Experimental Approach:** Surface plasmon resonance (SPR) assay was performed to validate the direct binding of BDB to PTP1B, and Lineweaver–Burk analysis of the enzyme kinetics was used to characterise the inhibition by BDB. Both in vitro enzyme-inhibition assays and SPR experiments were also conducted to study the selectivity exhibited by BDB towards four other PTP-family proteins: TC-PTP, SHP-1, SHP-2, and LAR. C2C12 myotubes were used to evaluate cellular permeability to BDB. Effects of BDB on insulin signalling, hypoglycaemia and hypolipidaemia were investigated in diabetic BKS db mice, after oral gavage. The beneficial effects of BDB on pancreatic islets were examined based on insulin and/or glucagon staining.

**Key Results:** BDB acted as a competitive inhibitor of PTP1B and demonstrated high selectivity for PTP1B among the tested PTP-family proteins. Moreover, BDB was cell-permeable and enhanced insulin signalling in C2C12 myotubes. Lastly, oral administration of BDB produced effective antidiabetic effects in spontaneously diabetic mice and markedly improved islet architecture, which was coupled with an increase in the ratio of β-cells to α-cells.

**Conclusion and Implications:** BDB application offers a potentially practical pharmacological approach for treating Type 2 diabetes mellitus by selectively inhibiting PTP1B.

KEYWORDS

bromophenol, PTP1B inhibitor, selectivity, cell permeability, oral bioavailability

**Abbreviations:** BDB, 3-bromo-4,5-bis(2,3-dibromo-4,5-dihydroxybenzyl)-1,2-benzenediol; BKS, C57BLKS/J; BKS db, BKS.Cg-Dock7$^{m+/+}$Lepr$^{db}$/J; CETSA, cellular thermal shift assay; CMC-Na, sodium carboxymethyl cellulose; DARTS, drug affinity responsive target stability; EDC, N-ethyl-N′-(dimethylaminopropyl)-carbodiimide; FBG, fasting blood glucose; FFA, free fatty acid; GSA, glycosylated serum albumin; HDL-C, HDL-cholesterol; IDF, International Diabetes Federation; IR, insulin receptor; IRS, insulin receptor substrate; ITT, insulin tolerance test; LDL-C, LDL-cholesterol; NHS, N-hydroxysuccinimide; OGTT, oral glucose tolerance test; p-NPP, p-nitrophenyl phosphate; PTP1B, protein tyrosine phosphatase 1B; pTyr, phosphotyrosine; RBG, random blood glucose; SPR, surface plasmon resonance; T2DM, Type 2 diabetes mellitus; TC, total cholesterol; TG, triglyceride.

  

CAS, Grant/Award Number: QYZDB-SSW-DQC014; Key Research and Development Project of Shandong Province, Grant/Award Numbers: 2018GSF118200, 2018GSF118208; National Natural Science Foundation of China, Grant/Award Number: 81703354

## 1 | INTRODUCTION

Diabetes is a worldwide epidemic that poses a major threat to global public health (Zheng, Ley, & Hu, 2018). The ninth Diabetes Atlas released by the International Diabetes Federation (IDF, 2019) identifies Asia as the epicentre of the diabetes crisis, with China being the country most affected by diabetes. **Type 2 diabetes** mellitus (T2DM) accounts for 90–95% of diabetes mellitus, which is characterized by insulin resistance and/or inadequate insulin secretion (American Diabetes, 2018; Chatterjee, Khunti, & Davies, 2017). Although considerable progress has been made in elucidating the molecular mechanisms of T2DM, satisfactory treatment modalities for diabetes remain limited (Leroith & Accili, 2008; Mittermayer et al., 2015).

Protein tyrosine phosphatase (PTP) 1B (**PTP1B**) down-regulates **insulin** and **leptin** signalling by catalysing tyrosine dephosphorylation of **insulin receptor**s (IR), insulin receptor substrate (IRS), and **leptin receptor**s (Byon, Kusari, & Kusari, 1998; Kenner, Anyanwu, Olefsky, & Kusari, 1996; Zhang, Dodd, & Tiganis, 2015), and PTP1B is thus a favourable drug target in therapeutic interventions for obesity and T2DM (Johnson, Ermolieff, & Jirousek, 2002; Krishnan et al., 2018; Zhang & Zhang, 2007). Genetic evidence indicates that a silent heterologous single nucleotide polymorphism in exon8 and an insert variant in the 3′-UTR of *PTP1B* are associated with increased risk of developing T2DM, compared with the risk in people who carry the wild-type *PTP1B* gene (Di Paola et al., 2002; Mok et al., 2002). Mice in which the *PTP1B* gene is knocked out are healthy and fertile, and the mice exhibit increased insulin sensitivity and resistance to high-fat diet-induced obesity (Delibegovic et al., 2009; Elchebly et al., 1999; Haj, Zabolotny, Kim, Kahn, & Neel, 2005; Klaman et al., 2000). Because PTP1B is a highly validated therapeutic target, many academic institutions and pharmaceutical companies have invested substantially in developing low MW inhibitors of PTP1B, and although several natural and synthetic PTP1B inhibitors have been reported, the FDA has not yet approved any drug (Erbe et al., 2005; Ito, Fukuda, Sakata, Morinaga, & Ohta, 2014; Lantz et al., 2010; Zasloff et al., 2001). The main challenge has been to identify PTP1B inhibitors that exhibit high selectivity, cell permeability and oral bioavailability (Combs, 2010).

Discovery of lead compounds and new drugs from the ocean holds considerable potential for yielding favourable therapeutic options for diverse diseases (Malve, 2016). Marine red algae of the family *Rhodomelaceae* contain numerous bromophenol compounds, and many of these compounds can produce various biological effects, including cytotoxicity (Wu et al., 2015), antioxidant effects (Li, Li, Ji, & Wang, 2007), and inhibition of glucose 6-phosphate dehydrogenase (Mikami, Kurihara, Kim, & Takahashi, 2013). Notably, several of these compounds also exhibit PTP1B inhibitory activity, and ethanol extracts from the red alga *Rhodomela confervoides* lower fasting glucose levels in the rat model of streptozotocin-induced diabetes (Shi et al., 2008). Accordingly, 3-bromo-4,5-bis(2,3-dibromo-4,5-dihydroxybenzyl)-1,2-benzenediol (BDB, chemical structure in Figure 1a), a natural bromophenol isolated from *R. confervoides*, was demonstrated to act as a potent PTP1B inhibitor (Cui, Shi, & Hu, 2011; Fan, Xu, & Shi, 2003; Shi et al., 2008). Considering these previous studies, we hypothesized that BDB could represent a promising therapeutic agent against T2DM. Therefore, in this study, we aimed to elucidate the characteristics of the inhibition of PTP1B, by BDB and to evaluate the hypoglycaemic and hypolipidaemic effects of BDB in spontaneously diabetic mice by using oral gavage. Moreover, we sought to examine the protective effects of BDB on pancreatic β-cells.

### What is already known

- 3-Bromo-4,5-bis(2,3-dibromo-4,5-dihydroxybenzyl)-1,2-benzenediol (BDB) is found in marine red algae and inhibits protein tyrosine phosphatase 1B.

### What this study adds

- BDB is shown to be a selective and cell-permeable inhibitor of PTP1B.
- Oral administration of BDB prevents hyperglycaemia in diabetic mice and concurrently improves islet architecture.

### What is the clinical significance

- BDB could emerge as a clinical drug candidate for T2DM treatment in the near future.

## 2 | METHODS

### 2.1 | In vitro enzyme-inhibition assay

The inhibitory effects of BDB on PTP1B and TC-PTP were assayed using p-nitrophenyl phosphate (p-NPP) as the substrate; the buffer solution contained 10-mM Tris–HCl (pH 7.5), 25-mM NaCl, 1-mM

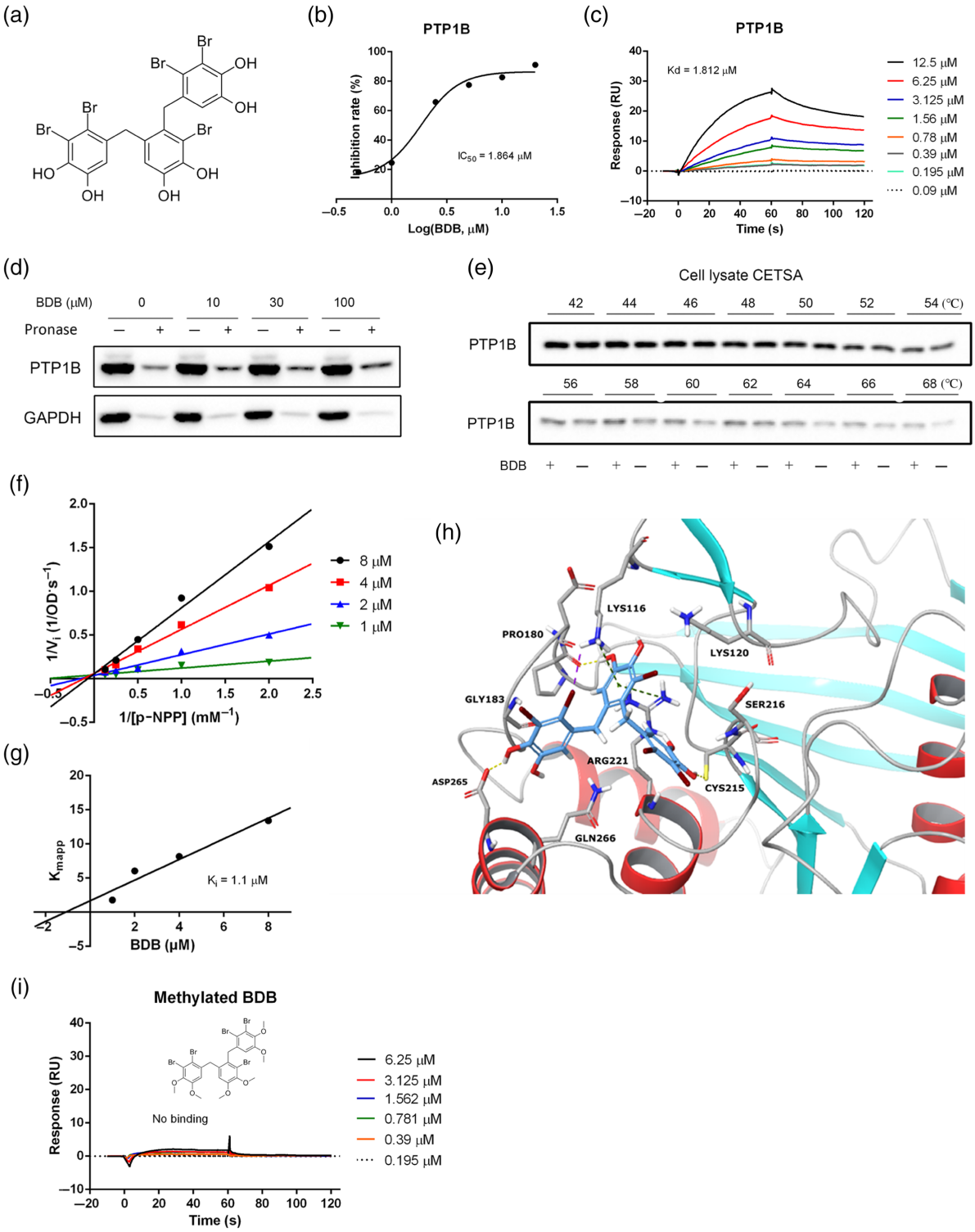


**FIGURE 1** Chemical structure and PTP1B inhibitory activity of BDB. (a) Chemical structure of BDB. (b) $IC_{50}$ of BDB inhibitory activity against PTP1B. Data are shown by plotting relative inhibition rate of PTP1B against log values of inhibitor concentration. (c) SPR characterization of binding affinity between BDB and PTP1B, which was immobilized on a CM5 chip. (d) Drug affinity responsive target stability (DARTS) assay performed using whole-cell lysates of C2C12 skeletal muscle cells, which were pretreated with 10-μM BDB. (e) Cellular thermal shift assay (CETSA) performed using lysates of C2C12 myotubes, which were exposed to 100-μM BDB. (f) Lineweaver–Burk analysis of PTP1B inhibition by BDB, which was applied at 1-, 2-, 4-, and 8-μM BDB; the reciprocal of reaction velocity ($1/V_i$) is plotted against the reciprocal of substrate concentration (1/[p-NPP]). (g) $K_i$ of BDB inhibitory activity against PTP1B. Data are shown by plotting $K_{mapp}$ values against the inhibitor concentrations. (h) Mode of BDB binding to PTP1B active site (PDB code 2HNP). The inhibitor BDB and key residues of PTP1B are shown in a capped stick representation. Carbon is shown in green for ligands and grey for PTP1B, oxygen is in orange, and bromine is in red. (i) SPR analysis of binding affinity between methylated BDB and PTP1B

EDTA, and 1-mM DTT, and the assay was performed as follows: 1 μl of enzyme (1 mg·ml$^{-1}$) and 1 μl of compounds (10-mM stock solution in DMSO) were added to 10 μl of 50-mM p-NPP in 88 μl of buffer solution in 96-well plates and the reaction mixture was incubated for 30 min at 37°C. The amount of p-nitrophenol, the catalytic product, was determined by measuring the 405-nm absorbance in a microplate reader. The inhibitory effects of the tested compounds are shown as the concentration that inhibited 50% of PTP1B enzyme activity ($IC_{50}$). Assays for SHP-1, SHP-2, and LAR were performed using OMFP as the substrate.

## 2.2 | Lineweaver–Burk analysis

BDB and human $PTP1B_{1-321}$ recombinant protein were preincubated at room temperature for 5 min, and then reaction mixtures (in 96-well plates) containing 10-mM Tris–HCl (pH 7.5), 25-mM NaCl, 1-mM EDTA, 1-mM DTT, and a series of p-NPP concentrations were incubated at 37°C for 10 min; subsequently, the p-nitrophenol content was determined by measuring the 405-nm absorbance. In the presence of 1-, 2-, 4-, and 8-μM BDB, the 1/[S] (mM$^{-1}$) and 1/[V] (1/OD·s$^{-1}$) values were determined from the substrate concentration and initial reaction rate, respectively, which were then plotted on the *x*-axis and *y*-axis. The enzyme inhibition type was identified from the intersection characteristics of the linear-regression lines.

## 2.3 | Surface plasmon resonance assay

Surface plasmon resonance (SPR) experiments were conducted using a Biacore T200 SPR spectrometer. For surface treatment of the CM5 sensor chip, PTP1B protein was immobilized on the chip by Amine Coupling Kit (BR-1000-50, GE Healthcare). First, the chip was activated by injecting a 1:1 mixture of 0.2-M N-ethyl-N′-(dimethylaminopropyl)-carbodiimide (EDC) and 0.05-M N-hydroxysuccinimide (NHS) for 420 s at a flow rate of 10 μl·min$^{-1}$; the PTP1B protein was diluted in 10-mM sodium acetate buffer (pH 5.0) to 10 μg·ml$^{-1}$, and ultimately ∼10,000 response units (RUs) were immobilized. Next, 1-M ethanolamine (pH 8.5) was applied for 7 min at a flow rate of 10 μg·ml$^{-1}$ to block excess reactive esters on the matrix. For use as the reference, the flow cell was subject to the aforementioned activation, immobilization, and blocking steps, but no protein was injected.

For kinetic analysis of small molecules and their corresponding protein interactions, the small molecules were prepared as 10-mM stock solutions in DMSO and then diluted in PBS-P20 buffer containing 5% DMSO. All compounds were injected into the protein-immobilized and reference flow cells for 60 s, which was followed by the allotted dissociation time of 60 s. To correct for the excluded volume effect, we used a series of DMSO calibration solutions. For kinetic evaluations, the reference data and blank data were subtracted by using the Biacore T200 evaluation software, with the solvent correction being performed concomitantly, after which curve-fitting (global fitting, 1:1 model) was performed for the entire dataset. For the layout of all the graphical data, we used GraphPad Prism 6.01 software (GraphPad Software, RRID: SCR_002798).

## 2.4 | Cell culture and western blotting

C2C12 myoblasts (ATCC, Cat# CRL-1772, RRID: CVCL_0188) were purchased from ATCC (Manassas, VA, USA) and cultured in DMEM supplemented with 10% FBS. The cells were generally seeded into six-well plate at 4 × $10^5$ cells per well, and at 90% confluence, the growth medium was changed to DMEM containing 10% horse serum (HS) to induce differentiation. After 4 days of differentiation, C2C12 skeletal muscle cells were starved overnight in serum-free DMEM and then treated for 8 h with BDB at different concentrations and either not stimulated or stimulated with insulin (100 nM) for 5 min.

Cells were lysed with RIPA buffer containing fresh PMSF, and after determining the total protein concentrations of the lysates by using a BCA kit, proteins were separated using SDS-PAGE and transferred to PVDF membranes. To assess the phosphorylation levels of insulin receptor substrate 1 (IRS1) and **Akt**, membranes were blocked with 5% skim milk and incubated with primary antibodies overnight at 4°C and then with secondary antibodies for 1 h at room temperature. Immunoreactive bands were detected using Western ECL Substrate, and images were captured using a ChemiDoc™ XRS$^+$ System (Bio-Rad). To detect the total protein levels of IRS1 and Akt, membranes were washed with stripping buffer (Thermo) and immunoblotted as described above. Five independent experiments were performed. The antibody-based procedures used in this study comply with the recommendations made by the *British Journal of Pharmacology* (Alexander et al., 2018).

## 2.5 | HPLC analysis for measuring cell permeability

This HPLC-based experiment was performed as previously reported (das Neves, Sarmento, Amiji, & Bahia, 2012; Luo et al., 2018). Briefly, C2C12 skeletal muscle cells were pretreated with BDB (10 μM) for 8 h, fixed with methanol, lysed using sonication, and then centrifuged to obtain the supernatant. The supernatant was evaporated under reduced pressure, and then the precipitate was dissolved in methanol and subject to HPLC analysis (π-Nap, 75% methanol/H2O + 2% acetic acid). DMSO-treated cells were used as the negative control.

## 2.6 | Cellular thermal shift assay

Cellular thermal shift assay (CETSA) studies were performed based on the method described previously (Martinez Molina et al., 2013). For cell-lysate CETSA, C2C12 skeletal muscle cells were collected in 1× PBS containing fresh protease-inhibitor cocktail and then frozen and thawed thrice (with liquid nitrogen being used for freezing cells). The lysates were divided into two aliquots, and one aliquot was treated with 100-μM BDB and one with DMSO (control). After 20-min incubation at

room temperature, each lysate was divided into 14 fractions, which were heated at different temperatures (42–68°C) for 3 min and then cooled at room temperature for 3 min; lastly, the lysates were boiled, separated using SDS-PAGE, and immunoblotted for PTP1B.

For intact-cell CETSA, C2C12 myotubes were pretreated with BDB (10 μM) for 8 h and then heated and cooled as described above. After the cells were frozen and thawed twice, lysates were collected by means of centrifugation and analysed through western blotting.

## 2.7 | Drug affinity responsive target stability assay

To determine PTP1B stability under protease treatment, the drug affinity responsive target stability (DARTS) assay was performed as described previously (Pai et al., 2015). Differentiated C2C12 myotubes were lysed using M-PER buffer containing a protease-inhibitor cocktail, and cell lysates were diluted in TNC buffer (50-mM Tris–HCl, pH 8.0, 50-mM NaCl, and 10-mM $CaCl_2$) and then treated with BDB at different concentrations (10, 30, and 100 μM) or DMSO (control). After incubating the mixtures at room temperature for 30 min, pronase (12.5 $\mu g \cdot ml^{-1}$) was added, and the incubation was continued for another 15 min at room temperature. The reaction was terminated by adding the protease-inhibitor cocktail, and the lysates were boiled and analysed through western blotting with anti-PTP1B antibody (Cat# sc-133259, RRID: AB_2174955). GAPDH was used as a negative control.

## 2.8 | Animal studies

### 2.8.1 | Animals

All animal care and experimental procedures were performed according to the guidelines approved by the Institute of Oceanology committees for the care and use of laboratory animals (HAIFAJIZI-2013-3; approval date: December 09, 2013). Animal studies are reported in compliance with the ARRIVE guidelines (Percie du Sert et al., 2020) and with the recommendations made by the *British Journal of Pharmacology* (Lilley et al., 2020). Efforts were made to minimize animal suffering.

We purchased 4- to 6-week-old male BKS.Cg-Dock7$^{m+/+}$Lepr$^{db}$/J diabetic mice (BKS db mice, also called db/db mice; The Jackson Laboratory, stock number 000642; RRID: IMSR_JAX:000642) and their lean C57BLKS/J wild-type controls (BKS mice; The Jackson Laboratory, stock number 000662; RRID: IMSR_JAX:000662) from the Model Animal Research Centre of Nanjing University (Nanjing, China).

### 2.8.2 | Housing and husbandry

Mice were housed in specific-pathogen-free conditions (two mice per cage), under controlled temperature (24 ± 2°C) and humidity (50–60%) and a regular 12/12-h light/dark cycle, and allowed free access to a normal chow diet and water.

### 2.8.3 | Validity

BKS db mice replicate various aspects of human T2DM Phases I–III. The blood glucose level of the BKS-background diabetic mice increased uncontrollably with age, and their islet β-cells decreased substantially.

### 2.8.4 | Blinding

Drugs (vehicle, metformin, and different concentrations of BDB) were prepared and numbered by the designer. The operator was blinded to the drugs.

### 2.8.5 | Studies conducted using BKS db mice

After 1 week of acclimatization, plasma glucose levels of all mice were assessed to verify the diabetic status, and the diabetic mice were randomly divided into four groups ($n$ = 8): diabetic model group (BKS db, treated with sodium carboxymethyl cellulose [CMC-Na] solution), metformin-treatment group (metformin, 100 $mg \cdot kg^{-1}$ body $wt \cdot day^{-1}$), low-dose BDB-treatment group (BDB-L, 50 $mg \cdot kg^{-1}$ body $wt \cdot day^{-1}$), and high-dose BDB-treatment group (BDB-H, 100 $mg \cdot kg^{-1}$ body $wt \cdot day^{-1}$). Age-matched male BKS mice (treated with CMC-Na solution) were used as the normal control ($n$ = 8). All mice were given drugs orally for 9 weeks. However, one mouse from BKS db group died at the fifth week due to improper gastric administration during the experimental period ($n$ = 7 after the fifth week).

To measure the long-time and short-time fasting blood glucose (FBG) levels, mice were fasted for 12 and 6 h, respectively. Glucose levels were measured using tail-vein blood and a OneTouch UltraEasy glucometer (Johnson & Johnson, USA).

At the end of the experiment, mice were anaesthetized using 10% chloral hydrate, and then blood samples of all mice were collected through the venous plexus behind the eyeball. Serum was separated using centrifugation and stored at −80°C. Serum total cholesterol (TC), triglyceride (TG), LDL-cholesterol (LDL-C), HDL-cholesterol (HDL-C), and free fatty acid (FFA) levels were determined according to the instructions of the assay-kit manufacturer. Because of insufficient serum samples, the group size varied from five to eight, and detailed group size was shown in the figure legends. The mice were then killed, and tissues were removed immediately and fixed in 10% formalin for subsequent immunohistochemical staining.

### 2.8.6 | Oral glucose tolerance test and insulin tolerance test

Given the number of participants and duration of the oral glucose tolerance test (OGTT) and insulin tolerance test (ITT) experiments, six

mice were randomly chosen from each group for the following tests. After 6 weeks of treatment, glucose (1.5 $g \cdot kg^{-1}$) was administered using gavage for the OGTT experiment after starvation for 12 h. After 7 weeks of treatment, insulin (1 $U \cdot kg^{-1}$) was injected subcutaneously for the ITT experiment after fasting for 6 h. Blood glucose was measured using tail-vein blood at the specific times. The AUC was calculated from the data collected during the OGTT and ITT experiments.

### 2.8.7 | Immunohistochemistry

Pancreas from all treated mice were collected and fixed in 4% paraformaldehyde solution overnight at 4°C. Subsequently, paraffin-embedded pancreas sections were rehydrated and heated with sodium citrate buffer for antigen retrieval and then blocked with 10% goat serum; to block endogenous peroxidases, the sections were treated with 3% hydrogen peroxide solution. Next, the sections were incubated (overnight at 4°C) with following primary antibodies (from Abcam): guinea pig anti-insulin antibody (1:100, Cat# ab7842, RRID: AB_306130), rabbit anti-glucagon antibody (1:8,000, Cat# ab92517, RRID: AB_10561971), and rabbit anti-Ki67 antibody (1 $\mu g \cdot ml^{-1}$, Cat# ab15580, RRID: AB_443209). For colour development, we used the HRP-DAB or AP-Permanent Red system or both, and then captured as digital images, and the results analysed by using a Tissue FAXS System (TissueGnostics, AT). Samples that showed dark staining and sections that appeared damaged were excluded from the analysis, and the group size varied from five to six, and detailed group size was shown in the Figure 7 legend. The histological staining results were statistically analysed, in a blinded manner, by a technician from TissueGnostics.

### 2.9 | Synthetic scheme for BDB and methylated BDB

BDB and its methylated derivative (Compound 6) were synthesized as follows. First, vanillin was reacted with bromine in $CH_3OH$ at 0°C to obtain Compound 1 at 95% yield (Fürstner, Stelzer, Rumbo, & Krause, 2002). Compound 1 was methylated with $CH_3I$ in DMF to generate Compound 2 (Fürstner et al., 2002) (97% yield), and then Compound 2 was brominated a second time by using two equivalents of bromine in acetic acid at 70°C, which yielded Compound 3 (Ford & Davidson, 1993) (63% yield). Compound 3 was reduced with $NaBH_4$ in methanol at 0°C to obtain an alcohol, Compound 4 (93% yield), and in the presence of $AlCl_3$, Friedel and Crafts reaction of Compound 4 with 1,2-dimethoxybenzene generated an intermediate compound, Compound 5 (90% yield). Compound 5 was reacted with bromine in $CH_2Cl_2$ at room temperature to generate Compound 6 (81% yield). BDB was obtained at 92% yield (purity >99%) by removing the methyl groups from Compound 6 with $BBr_3$ at 0°C.

The following synthetic scheme was used:

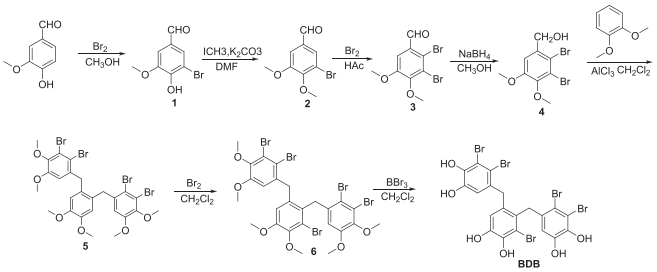


The structural-elucidation data were as follows:

Methylated BDB (Compound 6): m.p. 178–180°C; $^1$H NMR (500 MHz, $CDCl_3$) δ: 6.60 (s, 1H, Ar*H*), 6.45 (s, 1H, Ar*H*), 6.14 (s, 1H, Ar*H*), 4.20 (s, 2H, Ar$CH_2$Ar), 3.96 (s, 2H, Ar$CH_2$Ar), 3.88 (s, 3H, O$CH_3$), 3.80 (s, 6H, O$CH_3 \times 2$), 3.79 (s, 3H, O$CH_3$), 3.71 (s, 3H, O$CH_3$), 3.58 (s, 3H, O$CH_3$); $^{13}$C NMR (125 MHz, $CDCl_3$) δ: 152.4, 152.3, 152.2, 146.5, 146.0, 145.6, 136.0, 135.4, 135.2, 129.9, 122.8, 122.1, 121.7, 118.1, 117.5, 114.0, 113.8, 111.9, 60.5, 60.4, 56.2, 56.1, 42.1, 40.5. HR-EIMS m/z 831.7531 $[M]^+$, Calc. 831.7527.

BDB: $^1$H NMR (500 MHz, acetone-$d_6$) δ: 6.56 (s, 1H, Ar*H*), 6.50 (s, 1H, Ar*H*), 6.21 (s, 1H, Ar*H*), 4.05 (s, 2H, Ar$CH_2$Ar), 3.78 (s, 2H); $^{13}$C NMR (125 MHz, acetone-$d_6$) δ: 145.7, 145.6, 145.2, 144.0, 143.6, 133.0, 131.9, 129.3, 117.0, 116.5, 129.3, 115.1, 115.0, 114.0, 113.9, 41.0, 40.2. HR-EIMS m/z 742.6543 $[M]^+$, Calc. 742.6551.

### 2.10 | Data and statistical analyses

The data and statistical analysis comply with the recommendations of the *British Journal of Pharmacology* on experimental design and analysis in pharmacology (Curtis et al., 2018). Data were analysed in a blinded manner. Sample size (animal experiments) was planned based on our previous study on bromophenol compounds (Li et al., 2019). Group size was equal at design. However, in certain cases, adequate blood samples or pancreas sections were not obtained during testing, which explains the small sample size for recordings conducted with BDB. In the analysis of band density in western blotting, data were normalized to the internal control to exclude unwanted sources of variation. No data transformation was performed, and no outliers were removed in data analysis and presentation.

Results are presented as the means ± SEM. Statistical analysis was performed only when each group contained at least $n = 5$ independent samples, and the analysis was performed using one-way ANOVA followed by Tukey's post hoc test between control and various drug-treated groups. Tukey tests were conducted only when $F$ achieved a $P$ value of <0.05 and there was no significant variance inhomogeneity. Data from small group sizes of $n < 5$ were not subjected to statistical analysis. The declared group size is the number of independent values, and statistical analysis was performed using these independent values. Values were considered significant at $P < 0.05$, and this holds for the data shown later in Section 3. Analyses were performed using GraphPad Prism 6.01 software.

## 2.11 | Materials

The following reagents were from commercial sources: DMEM containing high-concentration glucose, penicillin–streptomycin, FBS, and HS, Hyclone (South Logan, UT, USA); EDTA-free protease-inhibitor cocktail and pronase, Roche (Basel, Switzerland); M-PER buffer, Thermo Fisher Scientific (Waltham, MA, USA); metformin, insulin, and CMC-Na, Sigma-Aldrich (St. Louis, MO, USA); Series S CM5 sensor chips, EDC, NHS, PBS-P20 buffer, 1.0-M ethanolamine-HCl (pH 8.5), and maintenance kit, GE (Mississauga, ON, Canada); DMSO and sodium acetate, Solarbo (Beijing, China); IRS1 antibody (Cat# 2382, RRID: AB_330333), Akt antibody (Cat# 9272, RRID: AB_329827), and phospho-Akt (Ser473) rabbit mAb (Cat# 4060, RRID: AB_2315049), Cell Signaling Technology (Danvers, MA, USA); anti-phospho-IRS1 (Tyr608)

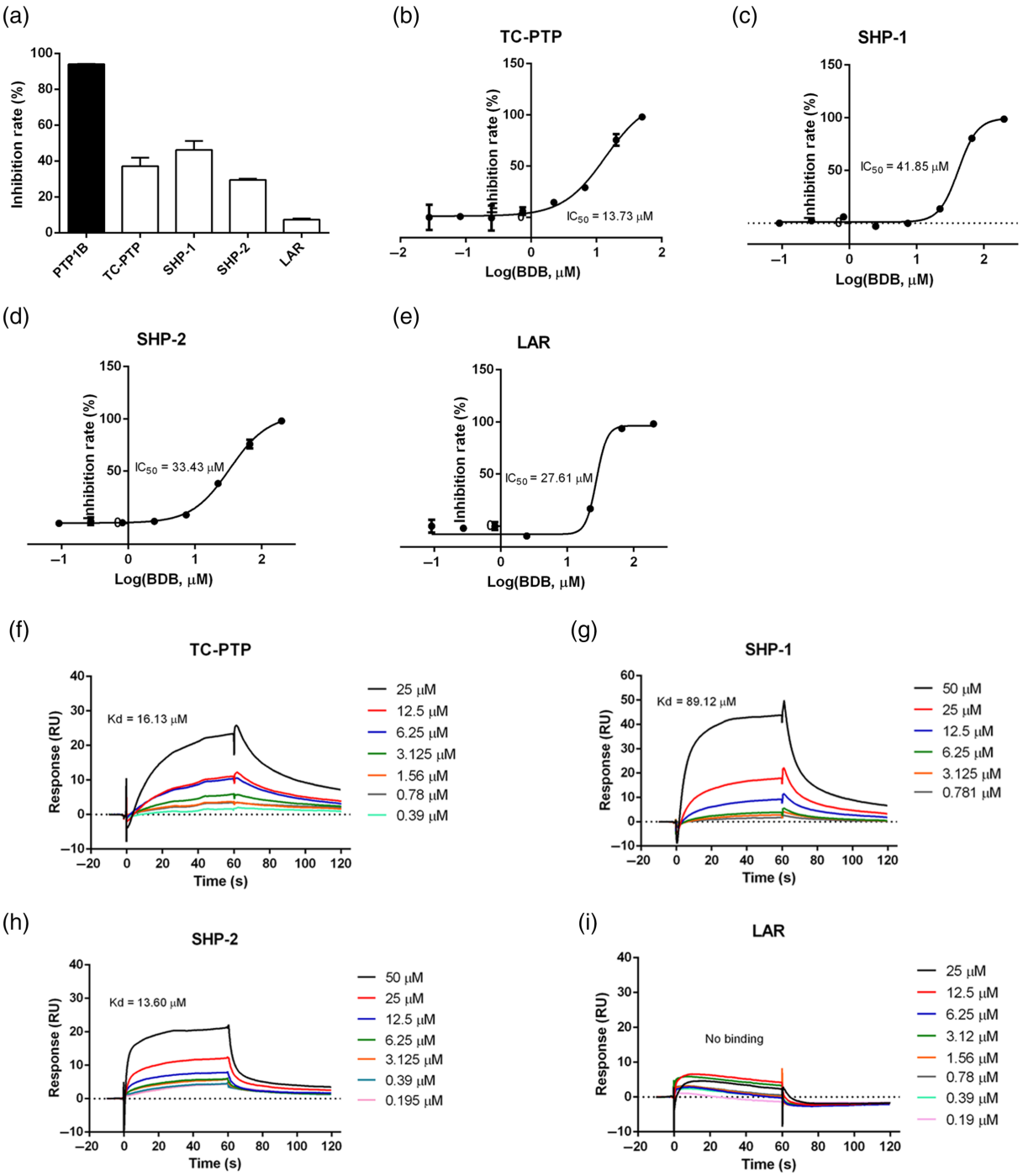


**FIGURE 2** Selectivity exhibited by BDB towards PTP1B and four other PTP-family proteins. (a) Inhibition by BDB (20 $\mu g \cdot ml^{-1}$) of PTP1B, TC-PTP, SHP-1, SHP-2, and LAR. (b–e) $IC_{50}$ values of BDB inhibitory activity against TC-PTP (b), SHP-1 (c), SHP-2 (d), and LAR (e). (f–i) SPR characterization of binding affinity between BDB and TC-PTP (f), SHP-1 (g), SHP-2 (h), and LAR (i), which were individually immobilized on CM5 chips

antibody (Cat# 09-432, RRID: AB_1163457), Millipore (Bedford, MA, USA); insulin antibody (Cat# ab7842, RRID: AB_306130), glucagon antibody (Cat# ab92517, RRID: AB_10561971), and Ki67 antibody (Cat# ab15580, RRID: AB_443209), Abcam (Cambridge, MA, USA); GAPDH antibody (Cat# 60004-1-Ig, RRID: AB_2107436), Proteintech (Wuhan, China); BCA Protein Assay Kit, Thermo (Waltham, MA, USA); Western ECL Substrate, Bio-Rad (Hercules, CA, USA); and TG, TC, LDL-C, HDL-C, and FFA assay kits and glycosylated serum protein assay kit, Nanjing Jiancheng Bioengineering Institute (Nanjing, China). Recombinant hPTP1B$_{1-321}$ protein was purified in our laboratory. Recombinant TC-PTP, SHP-1, SHP-2, and LAR proteins were from Sino Biological (Beijing, China).

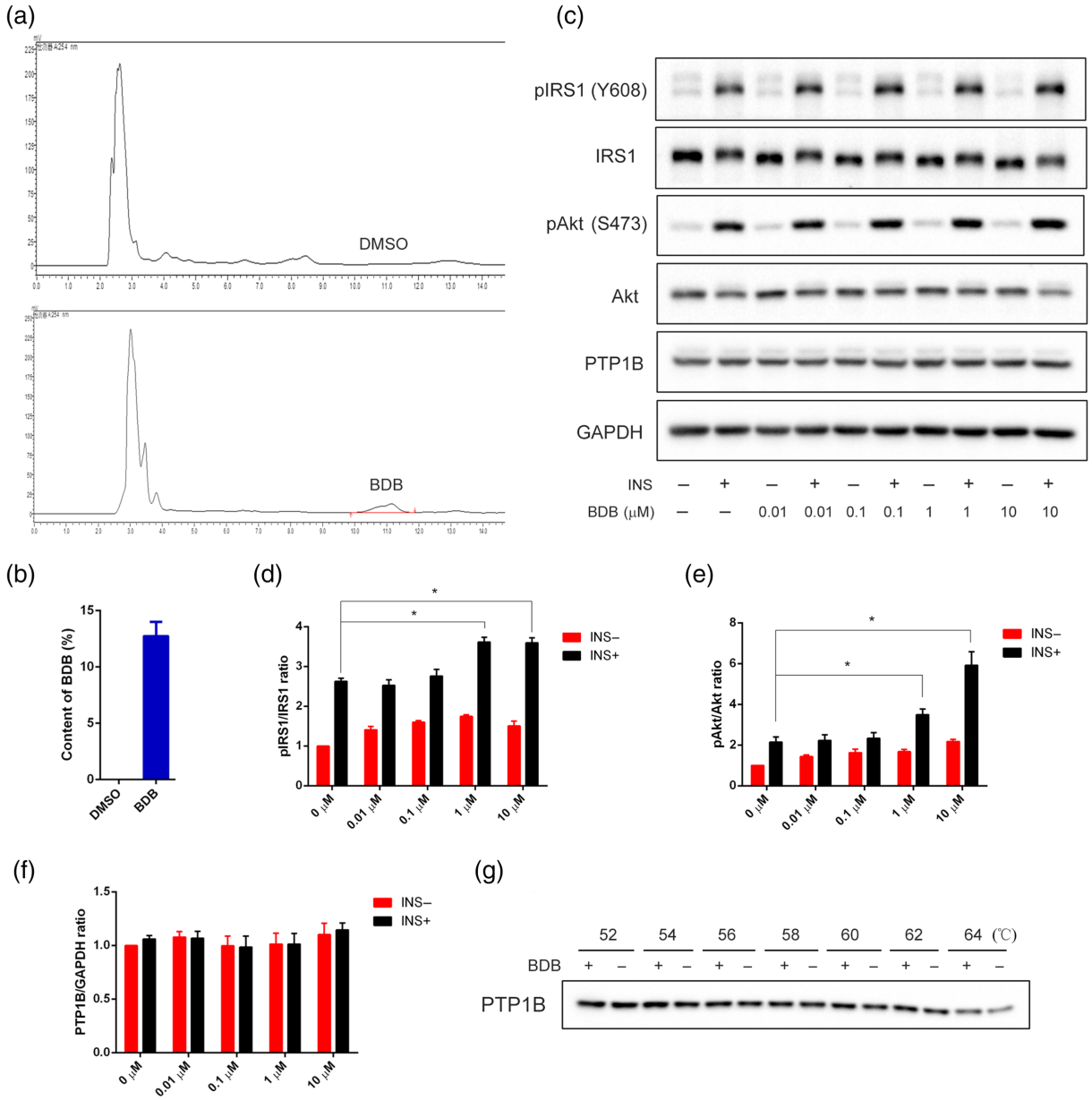


**FIGURE 3** BDB is cell permeable in C2C12 skeletal muscle cells. (a) HPLC analysis of DMSO- and BDB-treated C2C12 myotube lysates. Differentiated C2C12 myotubes were serum-starved overnight and then treated with DMSO or BDB (0.1 μmol) for 8 h. Subsequently, the myotubes were washed and fixed with methanol, and then cells were scraped and collected for HPLC analysis. (b) Uptake ratio of BDB in C2C12 myotubes. The amount of BDB was calculated using the standard curve method. Values are expressed as the average of five independent replicates ($n$ = 5). (c) Effects of BDB on insulin signalling pathway. Serum-starved C2C12 myotubes were pretreated with BDB for 8 h and then exposed for 5 min to 100-nM insulin treatment in serum-free medium. Immunoblotting was used to detect IRS1/Akt phosphorylation and PTP1B protein. (d) Ratio of tyrosine-phosphorylated IRS1 to total IRS1. (e) Ratio of serine-phosphorylated Akt to total Akt. (f) Ratio of PTP1B to GAPDH (control). Data are expressed as means ± SEM from five independent replicates ($n$ = 5). *$P$< 0.05, significantly different as indicated. (g) Cellular thermal shift assay (CETSA) performed using intact C2C12 myotubes, which were pretreated with 10-μM BDB

### 2.12 | Nomenclature of targets and ligands

Key protein targets and ligands in this article are hyperlinked to corresponding entries in http://www.guidetopharmacology.org, the common portal for data from the IUPHAR/BPS Guide to PHARMACOLOGY (Harding et al., 2018), and are permanently archived in the Concise Guide to PHARMACOLOGY 2019/20 (Alexander, Fabbro et al., 2019a, 2019b).enzymes

## 3 | RESULTS

### 3.1 | BDB is a competitive inhibitor of PTP1B

Recombinant hPTP1B$_{1-321}$ was used for measuring the in vitro inhibitory activity of BDB. BDB potently inhibited PTP1B, with an $IC_{50}$ of 1.86 μM (Figure 1b). To exclude the possibility that false-positive data were generated from the in vitro enzyme assay, direct interaction

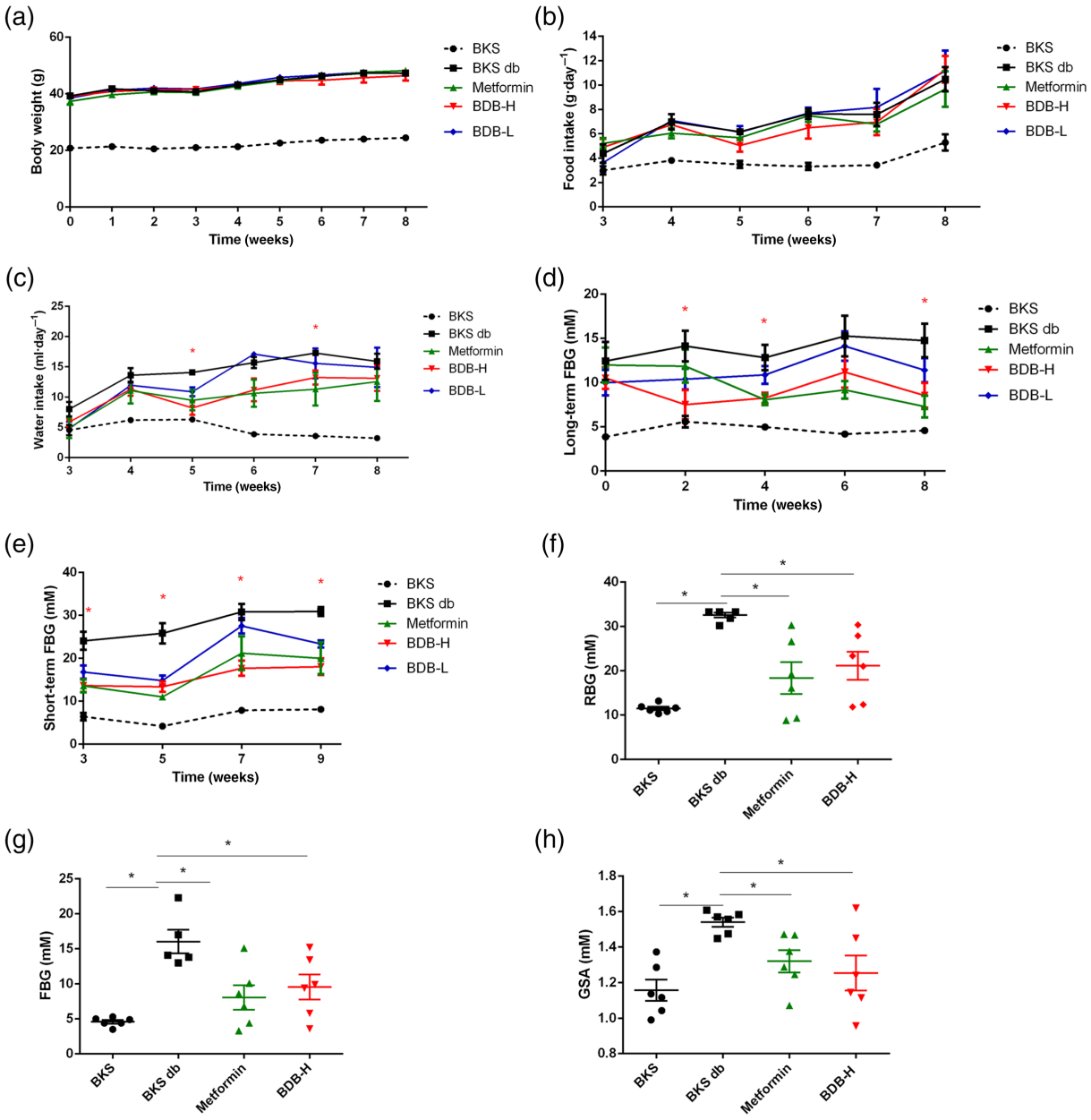


**FIGURE 4** Hypoglycaemic effect of BDB in diabetic BKS db mice. Animals were orally treated with BDB (50 or 100 mg·kg$^{-1}$, BDB-L, BDB-H, respectively) or metformin (100 mg·kg$^{-1}$) for 9 weeks. (a–c) Body weight (a), food intake (b), and water intake (c) of BKS db mice fed a normal chow diet and treated with/without BDB. (d, e) Plasma glucose levels of diabetic mice treated with vehicle, BDB, or metformin and of normal BKS mice treated with vehicle, after fasting for 12 h (d) or 6 h (e). $n$ = 8 for BKS, metformin, BDB-H, and BDB-L groups; for BKS db group, $n$ = 8 during the first to fourth week and $n$ = 7 during the fifth to ninth week. (f–h) Random blood glucose (RBG) levels (f), 12-h fasting blood glucose (FBG) levels (g), and serum glycosylated serum albumin (GSA) levels (h) at the end of 9-week treatment. $n$ = 6 for BKS, metformin, and BDB-H groups; for BKS db group, $n$ = 5 in RBG and FBG tests and $n$ = 6 in GSA test. Data are expressed as means ± SEM from the numbers of mice shown above. $^{*}P < 0.05$, (c, d, e) BDB-H group mice significantly different from vehicle-treated diabetic BKS db mice or (f, g, h) as indicated

between BDB and PTP1B was detected using SPR analysis, which revealed that BDB bound to PTP1B with an affinity of 1.812 μM and in a slow-on and slow-off manner (Figure 1c).

Low MW inhibitors can form ligand–protein complexes with their targets and thereby disrupt the function and increase the stability of target proteins. We used two target-engagement assays to investigate whether BDB binds to and enhances the stability of PTP1B. The results of DARTS assay showed that BDB treatment could protect PTP1B from pronase-induced proteolysis (Figure 1d), and the results of CETSA performed using C2C12 myotube lysates indicated that BDB protected PTP1B against temperature-dependent degradation (Figure 1e).

Next, the inhibitory type of BDB was studied through Lineweaver–Burk analysis of the enzyme reaction (Figure 1f); in the generated plot, the regression lines intersected on the *y*-axis, and whereas the $K_M$ values increased in a dose-dependent manner, the $V_{max}$ values did not change, indicating that BDB is a competitive inhibitor. The measured $K_i$ of BDB was 1.1 μM (Figure 1g).

To ascertain the manners in which BDB binds to PTP1B, we constructed 3D binding models in an open conformation of PTP1B (PDB code: 2HNP) through docking simulation (Figures S1 and 1h), which revealed that BDB is embedded in the active site and a dense network of hydrogen bonds is established between the phenolic hydroxyl groups of BDB and Pro180, Cys215, and Asp265 of PTP1B; moreover, Lys116 and Arg221 participate in the formation of cation–π interactions with the phenyl rings. Because of these multiple interactions, BDB can effectively self-adapt to the active site of the enzyme and function as a potent inhibitor.

Lastly, we again used SPR analysis to examine PTP1B interaction with a methylated derivative of BDB, which was synthesized in our laboratory. The methylated derivative did not bind to PTP1B (Figure 1i), which suggests that hydrogen bonding constitutes the main interaction force that maintains the binding of BDB and PTP1B.

## 3.2 | BDB is a specific inhibitor of PTP1B

Considering that PTP-family members contain a highly conserved catalytic domain, we next investigated the selectivity of BDB for PTP1B relative to four other PTPs: TC-PTP, SHP-1, SHP-2, and LAR. At 20 μg·ml$^{-1}$, BDB almost totally inhibited the activity of PTP1B but was markedly less effective against the other tested PTPs (<50% inhibited) (Figure 2a). The catalytic domain of TC-PTP shares 74% sequence identity with that of PTP1B (Figure S1), but the BDB $IC_{50}$ for TC-PTP (Figure 2b) was ~7.5-fold higher than that for PTP1B (Figure 1b). Moreover, the $IC_{50}$ values for SHP-1, SHP-2, and LAR were all higher than that for TC-PTP (Figure 2c–e), demonstrating that BDB was a specific inhibitor of PTP1B.

To confirm this selectivity of BDB, we immobilized these four PTPs on CM5 chips and performed SPR analysis. The affinity of BDB

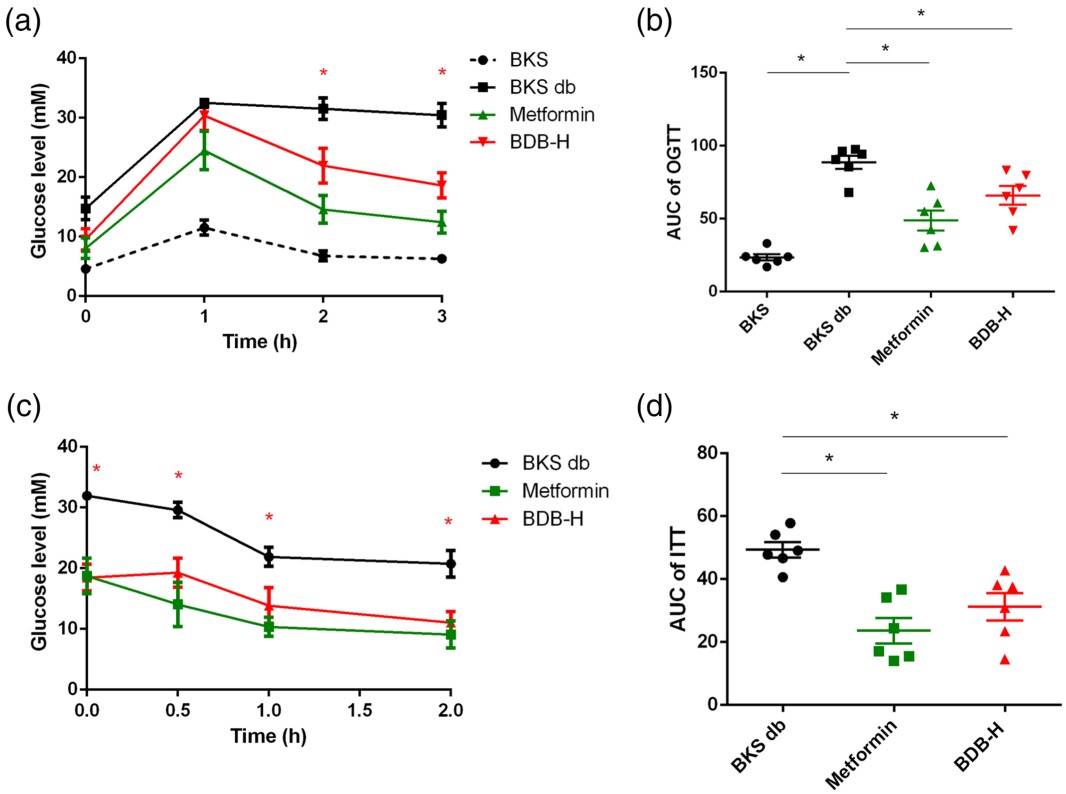


**FIGURE 5** Effect of BDB treatment on glucose intolerance and insulin resistance in diabetic mice. (a–d) Glucose tolerance (a) and insulin sensitivity (c) were measured using OGTT and ITT, respectively, in diabetic mice treated with/without BDB for 7 weeks. The AUC is shown on the right for OGTT (b) and ITT (d). Data are presented as means ± SEM ($n$ = 6). $^*P < 0.05$, (a, c) BDB-H group mice significantly different from vehicle-treated diabetic BKS db mice or (b, d) as indicated

binding to TC-PTP (Figure 2f), was ~8.9-fold lower than the affinity of BDB binding to PTP1B (Figure 1c). Similarly, BDB exhibited considerably lower binding affinity for SHP-1 and SHP-2 than PTP1B (Figure 2g,h) and, furthermore, showed no detectable binding to LAR (Figure 2i).

### 3.3 | BDB is cell permeable in C2C12 skeletal muscle cells

To function at cellular and whole-animal levels, BDB must penetrate the cell membrane, we therefore, assessed the cell-membrane permeability of BDB. First, we calculated the theoretical octanol–water partition coefficient to predict the lipophilicity of BDB. The theoretical cLogP was 6.94, which indicated preferential distribution of BDB into a hydrophobic environment rather than a hydrophilic environment; thus, BDB is likely to pass through the cell membrane. Next, we exposed C2C12 skeletal muscle cells to 10-μM BDB for 8 h and then used HPLC to measure the content of BDB in cell lysates (Figures S3 and 3a). The average ratio of BDB in the cell lysates in the five independent repetitions of the experiment is shown in Figure 3b, and indicates that BDB successfully passed through the cell membrane and accumulated intracellularly.

Given that BDB demonstrated the ability to cross the plasma membrane, we next examined the activity of BDB as a PTP1B inhibitor in whole cells. We used immunoblotting and analysed the

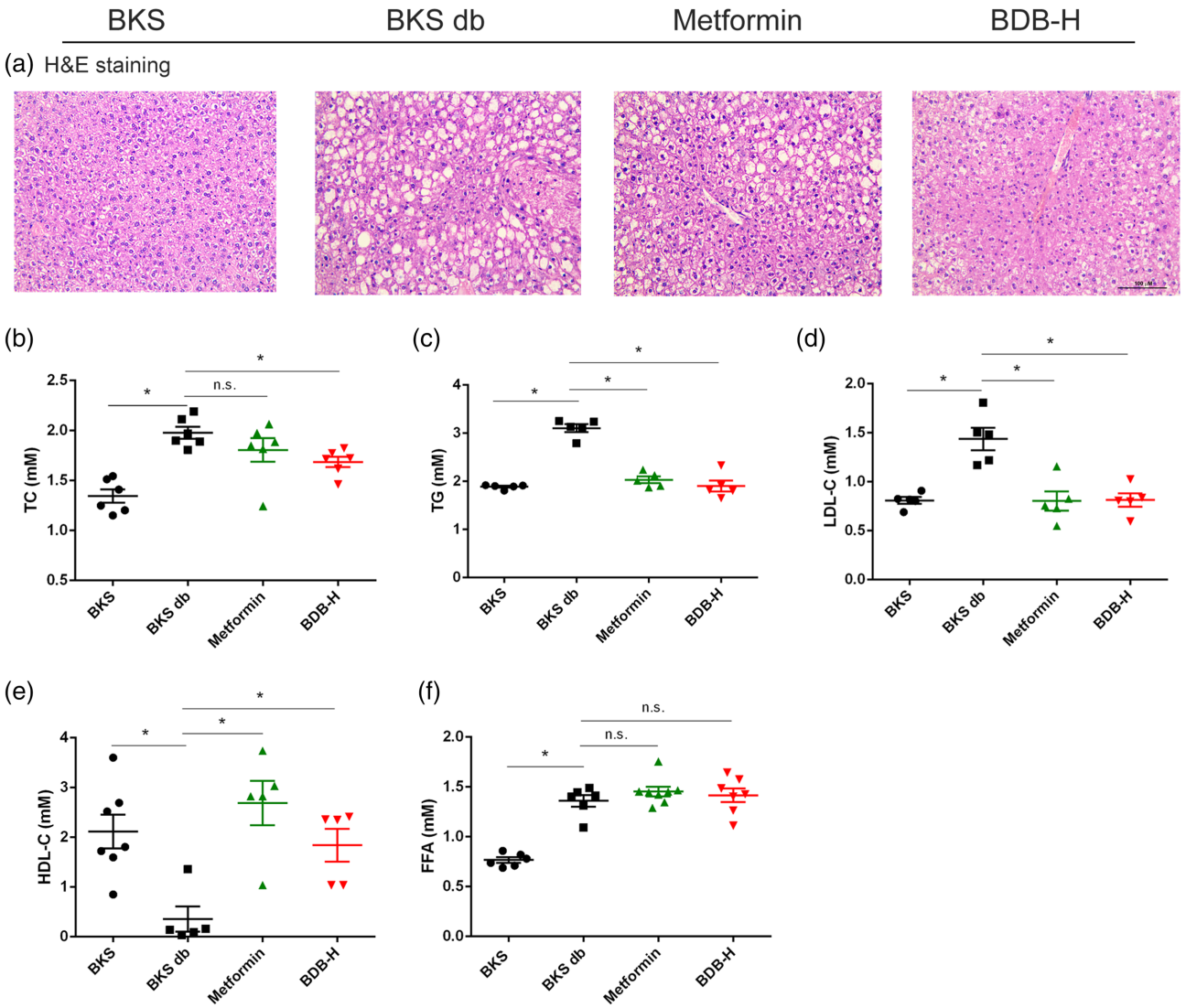


**FIGURE 6** Effects of BDB on dyslipidaemia in diabetic mice. (a) H&E staining of liver after 9-week treatment with vehicle in normal BKS mice or with vehicle, metformin, or high-dose BDB in diabetic BKS db mice (*scale bar*, 100 μM). (b–f) Mouse serum was prepared at the end of the ninth week and used for determining total cholesterol (TC, b), triglyceride (TG, c), LDL-cholesterol (LDL-C, d), HDL-cholesterol (HDL-C, e), and circulating free fatty acid (FFA, f) levels. In TC test, $n = 6$; in TG and LDL-C tests, $n = 5$; in HDL-C test, $n = 7$ for BKS group, and $n = 5$ for BKS db, metformin, and BDB-H groups; and in FFA test, $n = 6$ for BKS and BKS db groups, $n = 8$ for metformin group, and $n = 7$ for BDB-H group. Data are presented as means ± SEM, from the numbers of mice shown above. $^{*}P < 0.05$, significantly different as indicated; n.s., not significant

phosphorylation level of Tyr608 of IRS1, one of the direct substrates of PTP1B, and Ser473 of Akt, a downstream effector of IRS1 (Figure 3c). Notably, after BDB treatment, insulin-stimulated phosphorylation of IRS1-Tyr608 was increased (Figure 3d), as was that of Akt-Ser473 (Figure 3e), although PTP1B levels were unaffected by BDB exposure (Figure 3f). These results suggest that BDB enhances insulin signalling directly without altering the protein level of PTP1B.

We also tested whether BDB can increase the thermal stability of PTP1B in intact cells; CETSA results indicated that BDB treatment effectively protects PTP1B protein from temperature-dependent degradation at the intact-cell level (Figure 3g).

### 3.4 | Oral administration of BDB prevents hyperglycaemia in diabetic BKS db mice

To evaluate the potential antidiabetic effect of BDB in vivo, we used genetically diabetic mice: BKS db mice (db/db mice). Mice were given

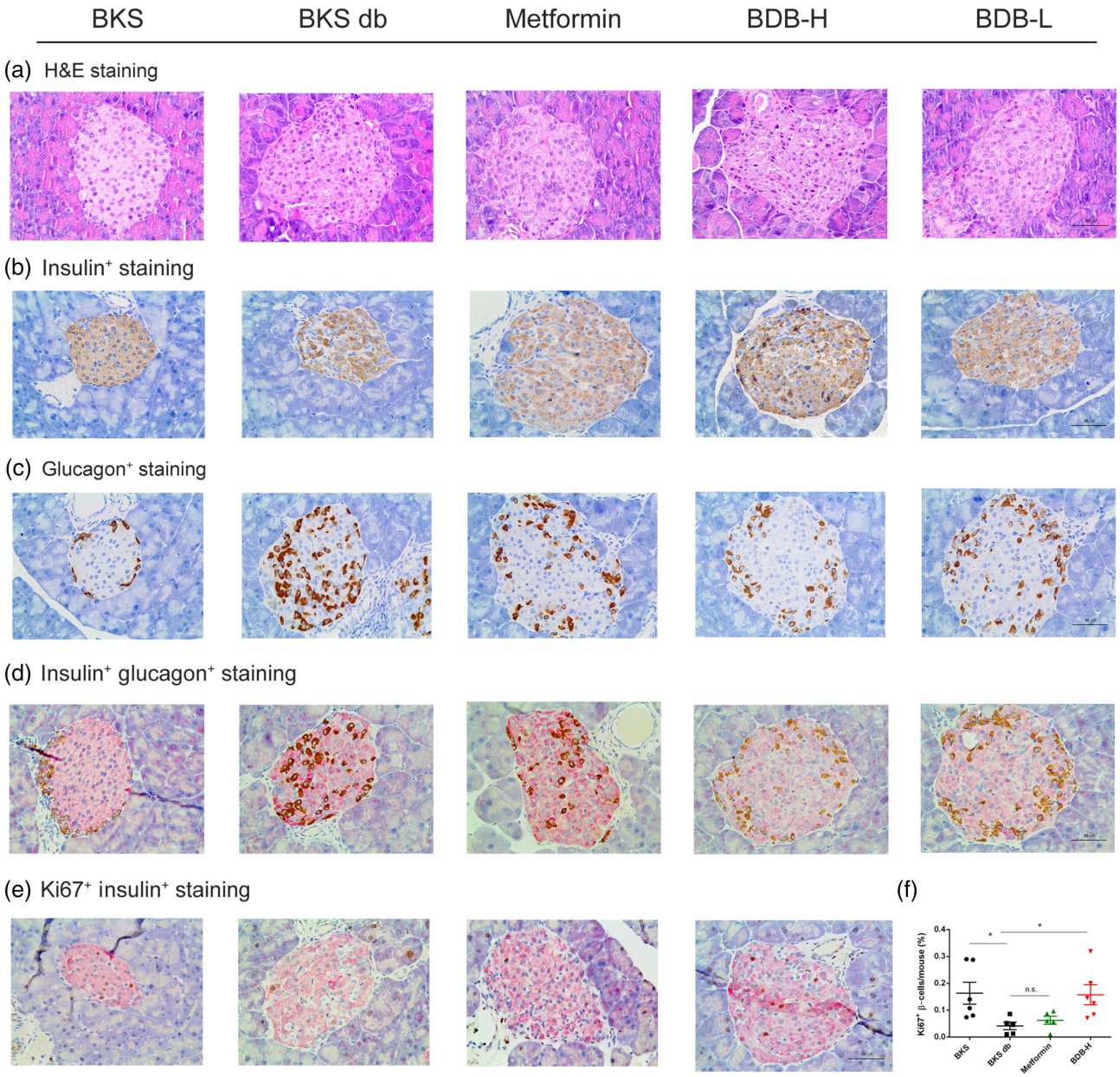


**FIGURE 7** Effects of BDB on pancreatic islet architecture in diabetic mice. After 9-week treatment of diabetic BKS db mice were treated with vehicle, metformin, or BDB, the pancreas was isolated, embedded in paraffin, and sectioned. Control: sections of pancreas are from normal BKS mice treated with vehicle. (a–e) H&E staining (a), insulin immunostaining (b), glucagon immunostaining (c), insulin and glucagon double-immunostaining (d), and insulin and Ki67 double-immunostaining (e) of pancreas from BKS mice treated with vehicle or from BKS db mice treated with vehicle, metformin, or BDB for 9 weeks (*scale bar*, 100 μm). (f) Percentage of Ki67-positive beta cells. $n = 6$ for BKS and BDB-H groups, and $n = 5$ for BKS db and metformin groups. Data are shown as means ± SEM from the numbers of mice shown above. $^{*}P < 0.05$, significantly different as indicated; n.s., not significant

BDB (50 and 100 mg·kg$^{-1}$ ·day$^{-1}$) orally for 9 weeks, and another group of mice was treated with metformin (100 mg·kg$^{-1}$ day$^{-1}$), as the positive control.

Diabetic mice are characterized by obesity, polyphagia, and polyuria. During the 9 weeks of treatment, BDB did not affect either body weight or food intake of the diabetic mice (Figure 4a,b). However, water intake of the mice in the BDB-treatment group showed a decreasing tendency starting from the fifth week (Figure 4c) and was significantly decreased at the fifth and seventh week.

Long-time and short-time fasting glucose levels were significantly decreased starting from the second week of high-dose BDB treatment (Figure 4d,e). Metformin effectively lowered the blood glucose level from the third week onwards, which was 1 week later than the BDB treatment. At the end of the ninth week, random blood glucose (RBG) levels and 12-h FBG levels were measured, showing that BDB treatment led to significant glycaemic control in the diabetic mice (Figure 4f,g). Moreover, serum glycosylated serum albumin (GSA) levels were decreased at the ninth week of BDB treatment (Figure 4h).

To examine the effects of BDB on glucose tolerance and insulin sensitivity, OGTT and ITT were performed: BDB improved glucose clearance in diabetic mice, with the quantified data showing that the AUC was decreased by ~25.6% (Figure 5a,b). BDB treatment also significantly decreased insulin resistance in BKS db mice, as indicated by the ~36.7% decrease in the AUC (Figure 5c,d).

Collectively, our results suggest that oral administration of BDB prevented hyperglycaemia and improved insulin sensitivity in diabetic BKS db mice.

### 3.5 | BDB treatment ameliorates hepatic steatosis and dyslipidaemia

As compared with non-diabetic control mice, vehicle-treated diabetic mice exhibited overt hepatic steatosis, with vacuolated and swollen hepatocytes present in liver sections (Figure 6a). BDB treatment ameliorated these hepatic disorders and caused significant reductions in circulating TC, TG, and LDL-C levels, relative to the levels after vehicle treatment (Figure 6b–d). Moreover, HDL-C levels were effectively increased after 9 weeks of BDB treatment (Figure 6e). However, BDB did not affect circulating FFA levels (Figure 6f). These results suggest that BDB treatment also mitigated the metabolic abnormalities associated with T2DM, such as hepatic steatosis and hyperlipidaemia.

### 3.6 | BDB treatment improves pancreatic islet architecture in BKS db mice

PTP1B inhibitors can effectively reduce blood glucose levels in diabetic animal models, but the long-term effect of PTP1B inhibition on pancreatic islets remains incompletely studied. Therefore, we performed multiple-antibody staining of pancreas and acquired digital images of whole-pancreas sections to characterize islet morphology and measure cell composition (Figures 7 and S4).

Pancreatic islet architecture and cell composition clearly differed between the non-diabetic and diabetic groups (Figure 7). In non-diabetic control mice, the islets harboured a large, tight, insulin-positive, beta cell core, surrounded by a layer of slightly glucagon-positive alpha cells, whereas the islets in vehicle-treated diabetic mice contained more glucagon-positive alpha cells, which penetrated the entire islet, including the central core (Figure 7b–d). Notably, 9 weeks of BDB treatment significantly increased the number of beta cells (Figure 7b), reduced the number of α-cells in the islets (Figure 7c), and increased the ratio of beta cells to alpha-cells (Figure 7d). More importantly, BDB treatment restored the distribution pattern of beta: alpha cells in the islets: the alpha cells in the islet core were markedly decreased and those at the islet edges were effectively increased (Figure 7d). Although islet PTP1B expression did not differ between non-diabetic and diabetic mice (Figure S4D), our results indicate that the efficacy of the low MW PTP1B inhibitor potentially extends beyond blood glucose control and helps improve islet architecture.

Lastly, we analysed beta cell proliferation in islets by double staining for Ki67, a marker of cellular proliferation, and insulin (Figure 7e). Relative to the level in healthy BKS mice, fewer Ki67-positive beta cells were present in the islets of vehicle-treated diabetic mice, but Ki67-positive beta cells were readily detected in the islets of BDB-treated BKS db mice (Figure 7f). These results indicate that BDB can enhance the islet architecture and beta cell mass by promoting the proliferation of beta cells.

## 4 | DISCUSSION AND CONCLUSIONS

Over the past decade, the phosphatase PTP1B has been regarded as a favourable drug target for therapeutic interventions designed for obesity and T2DM (He, Yu, Zhang, & Zhang, 2014). Consequently, much pharmaceutical research effort has been expended to identify low MW inhibitors of PTP1B for the treatment of T2DM and obesity-related metabolic diseases. However, most of the identified inhibitors are negatively charged phosphotyrosine (pTyr) mimics, such as phosphonates, carboxylic acids, and sulfamic acids, which exhibit poor selectivity for PTP1B and insufficient in vivo efficacy because of low cell permeability and bioavailability (Thareja, Aggarwal, Bhardwaj, & Kumar, 2012). To date, only five low MW PTP1B inhibitors have reached the clinical trial stage - ertiprotafib, TTP814, JTT-551, MSI-1436, and KQ-791, and no drug has as yet been approved for treatment.

To meet this challenge, we have focused on investigating low MW PTP1B inhibitors obtained from marine natural products and derivatives (Fan et al., 2003; Jiang, Guo, Shi, Guo, & Wang, 2013; Jiang, Shi, Cui, & Guo, 2012; Li et al., 2019; Luo et al., 2018; Luo, Jiang, Li, Jia, & Shi, 2019). BDB is a natural bromophenol isolated from the marine red alga *R. confervoides* (Fan et al., 2003). Here, we have identified BDB as a competitive inhibitor of PTP1B by using in vitro enzyme inhibition assays. Moreover, to eliminate any false-positive

data that might be obtained in enzymic reaction analyses, we used the SPR assay to examine the direct binding of BDB with PTP1B. The Biacore SPR method is a rapid, label-free, and real-time technique for detecting biomolecular interactions (Schasfoort, 2017), and continuous enhancement of the sensitivity of commercial SPR instruments has resulted in SPR becoming a well-established and necessary research tool for studying the binding of low MW compounds to proteins (Liao et al., 2017). The binding affinity between proteins and low MW compounds generally ranges from $10^{-3}$ to $10^{-6}$ M, and the affinity of BDB for PTP1B was measured to be $1.8 \times 10^{-6}$ M. This suggests that BDB is a potent PTP1B inhibitor.

The results of molecular dynamics simulations revealed that BDB is deeply embedded in the pocket of the PTP1B catalytic domain and that strong hydrogen-bonding interactions exist between BDB and the residues of PTP1B. Importantly, by using SPR to examine the interaction between a methylated derivative of BDB and PTP1B, we determined that the hydrogen bonds provide the main interaction force underlying the binding of BDB and PTP1B. Thus, it is likely that BDB inhibits PTP1B by competing with the substrate for interaction at the enzyme's catalytic domain, with the binding of BDB being mostly mediated by hydrogen bonding.

The results of docking analyses indicated that BDB interacts with the PTP1B residues Pro180, Cys215, and Asp265. Intriguingly, these residues are the same as the corresponding residues in TC-PTP (Figure S2). PTP-family proteins contain a highly conserved catalytic domain, and this is particularly relevant here in the case of TC-PTP, which shares 74% sequence identity with PTP1B in its catalytic domain. Moreover, the active sites of these two proteins are identical (Andersen et al., 2001; Johnson et al., 2002). Poor selectivity can cause target-related side effects, and selectivity is one of the major challenges faced in the development of PTP1B inhibitors. Nevertheless, we showed here that BDB acted as a specific inhibitor of PTP1B and further that BDB exhibited lower binding affinity for TC-PTP, SHP-1, and SHP-2 and showed no binding to LAR. The mechanism underlying this selectivity is unclear, and this could be addressed in future studies by performing 2D-HNMR and co-crystallization of BDB with PTP1B. However, currently, the selectivity exhibited by inhibitors towards closely related phosphatases remains to be explained.

PTP1B anchors on the cytoplasmic face of the endoplasmic reticulum through a C-terminal hydrophobic sequence (Frangioni, Beahm, Shifrin, Jost, & Neel, 1992) and catalyses protein dephosphorylation by means of its charged active site (Xiao et al., 2014). Several compounds have been found to inhibit PTP1B highly effectively in vitro, but poor cell permeability limits the ability of these compounds to reach their intracellular target. For example, many of the inhibitory compounds are highly charged or strongly polar because they contain pTyr mimetics, and thus, these compounds cannot pass through the cell membrane and access intracellular PTP1B. By contrast, BDB, unlike pTyr mimetics, is an uncharged compound, and its theoretical cLogP was calculated here to be 6.94; thus, BDB is expected to show preferential distribution into a hydrophobic rather than a hydrophilic milieu and is likely to pass through the cell membrane. Accordingly, our HPLC analysis of BDB accumulation in C2C12 myotubes yielded an average BDB ratio in the myotubes of nearly 13%, which indicates that BDB successfully passed through the cell membrane and accumulated intracellularly. However, a limitation of the HPLC method is that the nonspecific adsorption of BDB on the cell membrane cannot be excluded, and thus, we performed immunoblotting and intact-cell CETSA to further assess the ability of BDB to interact with intracellular PTP1B and enhance PTP1B-mediated insulin signalling. We were able to show that BDB protected intracellular PTP1B from temperature-dependent degradation and that BDB directly increased the phosphorylation levels of IRS1 and Akt, without altering the protein level of PTP1B. These results indicate that BDB is cell-permeable. However, high cLogP value could affect the solubility of BDB and, consequently, may influence the absorption of BDB. It will be essential to determine the pharmacokinetics of this inhibitor, measuring the absorption, distribution, and elimination of BDB in mice in further studies.

The in vivo efficacy of several PTP1B inhibitors does not always agree with their observed in vitro effects and pharmacodynamic studies on these inhibitors in diabetic animal models are crucial. More importantly, oral bioavailability is one of the major challenges encountered in the development of PTP1B inhibitors (Combs, 2010). In this study, we investigated the effects of long-term oral administration of BDB. BDB markedly reduced fasting glucose levels starting from the second week, and this demonstrated that the BDB effect was measurable 1 week earlier than the effect of metformin. OGTT results further showed that BDB increased the ability of diabetic mice to clear glucose, and ITT results showed that BDB notably decreased insulin resistance in BKS db mice. Taken together, our results indicated high bioavailability of BDB, and oral administration of BDB prevented hyperglycaemia and concurrently enhanced glucose tolerance and insulin sensitivity.

Dyslipidaemia, which affects ~50% of T2DM patients, is a risk factor for cardiovascular complications. Diabetic dyslipidaemia is characterized by a high plasma TG concentration, low HDL-C concentration, and high LDL-C concentration (Mooradian, 2009). We found that BDB markedly reduced the circulating levels of TC, TG, and LDL-C and effectively increased the level of HDL-C, which indicates that BDB exerted ameliorative effects on aberrant blood lipid levels.

Diabetes mellitus is a progressive disease in which beta cell counts start to decrease from as early as the diagnosis of pre-diabetes, and these cell numbers in pancreatic islets decrease at a rate of ~4% per year as the disease progresses (Halban et al., 2014; Wang et al., 2015). In T2DM patients, beta cell failure occurs as a result of de-differentiation, which results in the decrease in beta cell numbers (Halban et al., 2014). Given this new understanding of the mechanism of beta cell failure, identification of effective methods to reverse the de-differentiation of beta cells has emerged as the key to the treatment of diabetes mellitus. Among the currently approved oral hypoglycaemic drugs, insulin secretagogues can induce beta cell apoptosis (Maedler et al., 2005), and glinides can damage beta cell function (Takahashi et al., 2007). Moreover, long-term use of insulin sensitizers and glycosidase inhibitors does not help improve the function of beta cells (Halban et al., 2014). Therefore, there is an urgent need for effective therapeutic drugs to restore the numbers of beta cells in T2DM patients.

The role of PTP1B in regulating the insulin signalling pathway is widely recognized, but few investigations to date have focused on the function of PTP1B in pancreatic beta cells. A previous study showed that, relative to control mice, mice with *PTP1B* deletion in the pancreas displayed earlier impairment of glucose tolerance and attenuated glucose-stimulated insulin secretion under high-fat-diet feeding (Liu et al., 2014). However, highly contrasting results were obtained in another study in which isolated islets from 8-week-old *PTP1B*$^{-/-}$ mice showed enhanced glucose-stimulated insulin secretion (Fernandez-Ruiz, Vieira, Garcia-Roves, & Gomis, 2014), and pancreatic islets from *PTP1B*$^{-/-}$ mice also exhibited, relative to control, increased beta cell area, coupled with higher proliferation and lower apoptosis (Fernandez-Ruiz et al., 2014). In our experiments, we have used a low MW inhibitor of PTP1B to further investigate the precise role of PTP1B in regulating pancreatic beta cell mass. Intriguingly, BDB treatment improved pancreatic islet architecture and concurrently increased the percentage of beta cells and decreased percentage of alpha cells. Moreover, BDB administration increased the number of Ki67-positive beta cells, which implies that the treatment promoted beta cell proliferation. Thus, our study indicates that selective inhibition of PTP1B is not only beneficial for glycaemic control but also conducive to the proliferation and viability of pancreatic beta cells. A more recent study confirmed that the protective effect exerted by PTP1B on islets represents another mechanism of action of the enzyme: targeting of pancreatic islet PTP1B improved islet graft revascularization and transplant outcomes (Figueiredo et al., 2019). Collectively, these findings reveal that targeting PTP1B can improve the structure and function of diabetic islets.

As compared with kinase research, phosphatase research is still in its infancy. Several early studies led many to believe that phosphatases were "undruggable" targets because of the high conservation rate of their active site. Here, we have provided proof-of-concept results indicating that these challenges associated with active-site-directed inhibitors of PTP1B can be overcome. We have identified BDB as a specific PTP1B inhibitor that exhibits high cell permeability, and we have also presented evidence that BDB is orally bioavailable and exerts antidiabetic effects in a spontaneously diabetic mouse model and concurrently enhances glucose tolerance and insulin sensitivity in these mice. More importantly, we have reported that BDB improves pancreatic islet architecture and concomitantly increases beta cell numbers.

The current study also has some limitations. Additional investigations into the mechanism underlying BDB specificity for PTP1B and further testing of BDB selectivity by including additional PTPs and *PTP1B*-knockout cells/animals need to be addressed in further work. The pharmacokinetics and toxicity of BDB should also be evaluated in the mouse model.

In conclusion, this study has shown that oral administration of BDB successfully produced antidiabetic effects by selectively inhibiting PTP1B. Our study has also provided new insights into the role of PTP1B in pancreatic beta cells. Our hope is that BDB will emerge as a candidate drug for clinical treatment of T2DM in the near future.

## ACKNOWLEDGEMENTS

This work was supported by the National Natural Science Foundation of China (81703354), Key Research and Development Project of Shandong Province (2018GSF118200 and 2018GSF118208), Key Research Program of Frontier Sciences, CAS (QYZDB-SSW-DQC014), and National Program for Support of Top-notch Young Professionals, Fund of Taishan scholar project, Shandong Provincial Natural Science Foundation for Distinguished Young Scholars (JQ201722), NSFC-Shandong Joint Fund (U1706213), and Qingdao Marine Biomedical Science and Technology Innovation Center project (2017-CXZX01-1-1 and 2017-CXZX01-3-9).

## AUTHOR CONTRIBUTIONS

J.L. conceived, designed, and conducted this study. M.Z. and R.Y. performed the molecular docking. J.L. and B.J. drafted and revised the manuscript. C.L., S.G., L.W., and X.L. provided great help for the laboratory technique, experiments, and data analysis. D.S. provided the financial support and supervised the study. All authors reviewed the results and approved the final version of the manuscript.

## CONFLICT OF INTEREST

The authors declare no conflicts of interest.

## DECLARATION OF TRANSPARENCY AND SCIENTIFIC RIGOUR

This Declaration acknowledges that this paper adheres to the principles for transparent reporting and scientific rigour of preclinical research as stated in the *BJP* guidelines for Design & Analysis, Immunoblotting and Immunochemistry, and Animal Experimentation, and as recommended by funding agencies, publishers, and other organizations engaged with supporting research.

## ORCID

*Jiao Luo* https://orcid.org/0000-0003-4810-2009

## REFERENCES

Alexander, S. P. H., Fabbro, D., Kelly, E., Mathie, A., Peters, J. A., Veale, E. L., … CGTP Collaborators. (2019a). THE CONCISE GUIDE TO PHARMACOLOGY 2019/20: Catalytic receptors. *British Journal of Pharmacology*, *176*, S247–S296. https://doi.org/10.1111/bph.14751

Alexander, S. P. H., Fabbro, D., Kelly, E., Mathie, A., Peters, J. A., Veale, E. L., … CGTP Collaborators. (2019b). THE CONCISE GUIDE TO PHARMACOLOGY 2019/20: Enzymes. *British Journal of Pharmacology*, *176*, S297–S396. https://doi.org/10.1111/bph.14752

Alexander, S. P. H., Roberts, R. E., Broughton, B. R. S., Sobey, C. G., George, C. H., Stanford, S. C., … Ahluwalia, A. (2018). Goals and practicalities of immunoblotting and immunohistochemistry: A guide for submission to the *British Journal of Pharmacology*. *British Journal of Pharmacology*, *175*, 407–411. https://doi.org/10.1111/bph.14112

American Diabetes A. (2018). 2. Classification and diagnosis of diabetes: Standards of medical care in diabetes—2018. *Diabetes Care*, *41*, S13–S27. https://doi.org/10.2337/dc18-S002

Andersen, J. N., Mortensen, O. H., Peters, G. H., Drake, P. G., Iversen, L. F., Olsen, O. H., et al. (2001). Structural and evolutionary relationships among protein tyrosine phosphatase domains. *Molecular and Cellular*

*Biology*, *21*, 7117–7136. https://doi.org/10.1128/MCB.21.21.7117-7136.2001

Byon, J. C., Kusari, A. B., & Kusari, J. (1998). Protein-tyrosine phosphatase-1B acts as a negative regulator of insulin signal transduction. *Molecular and Cellular Biochemistry*, *182*, 101–108. https://doi.org/10.1023/A:1006868409841

Chatterjee, S., Khunti, K., & Davies, M. J. (2017). Type 2 diabetes. *Lancet*, *389*, 2239–2251. https://doi.org/10.1016/S0140-6736(17)30058-2

Combs, A. P. (2010). Recent advances in the discovery of competitive protein tyrosine phosphatase 1B inhibitors for the treatment of diabetes, obesity, and cancer. *Journal of Medicinal Chemistry*, *53*, 2333–2344. https://doi.org/10.1021/jm901090b

Cui, Y., Shi, D., & Hu, Z. (2011). Synthesis and protein tyrosine phosphatase 1B inhibition activities of two new synthetic bromophenols and their methoxy derivatives. *Chinese Journal of Oceanology and Limnology*, *29*, 1237–1242. https://doi.org/10.1007/s00343-011-0271-8

Curtis, M. J., Alexander, S., Cirino, G., Docherty, J. R., George, C. H., Giembycz, M. A., … Ahluwalia, A. (2018). Experimental design and analysis and their reporting II: Updated and simplified guidance for authors and peer reviewers. *British Journal of Pharmacology*, *175*, 987–993. https://doi.org/10.1111/bph.14153

das Neves, J., Sarmento, B., Amiji, M., & Bahia, M. F. (2012). Development and validation of a HPLC method for the assay of dapivirine in cell-based and tissue permeability experiments. *Journal of Chromatography. B, Analytical Technologies in the Biomedical and Life Sciences*, *911*, 76–83. https://doi.org/10.1016/j.jchromb.2012.10.034

Delibegovic, M., Zimmer, D., Kauffman, C., Rak, K., Hong, E. G., Cho, Y. R., … Bence, K. K. (2009). Liver-specific deletion of protein-tyrosine phosphatase 1B (PTP1B) improves metabolic syndrome and attenuates diet-induced endoplasmic reticulum stress. *Diabetes*, *58*, 590–599. https://doi.org/10.2337/db08-0913

Di Paola, R., Frittitta, L., Miscio, G., Bozzali, M., Baratta, R., Centra, M., et al. (2002). A variation in 3' UTR of hPTP1B increases specific gene expression and associates with insulin resistance. *American Journal of Human Genetics*, *70*, 806–812. https://doi.org/10.1086/339270

Elchebly, M., Payette, P., Michaliszyn, E., Cromlish, W., Collins, S., Loy, A. L., … Kennedy, B. P. (1999). Increased insulin sensitivity and obesity resistance in mice lacking the protein tyrosine phosphatase-1B gene. *Science*, *283*, 1544–1548. https://doi.org/10.1126/science.283.5407.1544

Erbe, D. V., Wang, S., Zhang, Y. L., Harding, K., Kung, L., Tam, M., … Tobin, J. F. (2005). Ertiprotafib improves glycemic control and lowers lipids via multiple mechanisms. *Molecular Pharmacology*, *67*, 69–77. https://doi.org/10.1124/mol.104.005553

Fan, X., Xu, N. J., & Shi, J. G. (2003). Bromophenols from the red alga *Rhodomela confervoides*. *Journal of Natural Products*, *66*, 455–458. https://doi.org/10.1021/np020528c

Fernandez-Ruiz, R., Vieira, E., Garcia-Roves, P. M., & Gomis, R. (2014). Protein tyrosine phosphatase-1B modulates pancreatic beta-cell mass. *PLoS ONE*, *9*, e90344. https://doi.org/10.1371/journal.pone.0090344

Figueiredo, H., Figueroa, A. L. C., Garcia, A., Fernandez-Ruiz, R., Broca, C., Wojtusciszyn, A., … Gomis, R. (2019). Targeting pancreatic islet PTP1B improves islet graft revascularization and transplant outcomes. *Science Translational Medicine*, *11*, eaar6294. https://doi.org/10.1126/scitranslmed.aar6294

Ford, P. W., & Davidson, B. S. (1993). Synthesis of varacin, a cytotoxic naturally occurring benzopentathiepin isolated from a marine ascidian. *The Journal of Organic Chemistry*, *58*, 4522–4523. https://doi.org/10.1021/jo00069a006

Frangioni, J. V., Beahm, P. H., Shifrin, V., Jost, C. A., & Neel, B. G. (1992). The nontransmembrane tyrosine phosphatase PTP-1B localizes to the endoplasmic reticulum via its 35 amino acid C-terminal sequence. *Cell*, *68*, 545–560. https://doi.org/10.1016/0092-8674(92)90190-N

Fürstner, A., Stelzer, F., Rumbo, A., & Krause, H. (2002). Total synthesis of the turrianes and evaluation of their DNA-cleaving properties. *Chemistr-A European Journal*, *8*, 1856–1871.

Haj, F. G., Zabolotny, J. M., Kim, Y. B., Kahn, B. B., & Neel, B. G. (2005). Liver-specific protein-tyrosine phosphatase 1B (PTP1B) re-expression alters glucose homeostasis of PTP1B−/− mice. *The Journal of Biological Chemistry*, *280*, 15038–15046. https://doi.org/10.1074/jbc.M413240200

Halban, P. A., Polonsky, K. S., Bowden, D. W., Hawkins, M. A., Ling, C., Mather, K. J., … Weir, G. C. (2014). β-cell failure in type 2 diabetes: Postulated mechanisms and prospects for prevention and treatment. *Diabetes Care*, *37*, 1751–1758. https://doi.org/10.2337/dc14-0396

He, R. J., Yu, Z. H., Zhang, R. Y., & Zhang, Z. Y. (2014). Protein tyrosine phosphatases as potential therapeutic targets. *Acta Pharmacologica Sinica*, *35*, 1227–1246. https://doi.org/10.1038/aps.2014.80

International Diabetes Federation. (2019). IDF Diabetes Atlas—Ninth Edition. Retrieved from https://idf.org/e-library/epidemiology-research/diabetes-atlas.html

Ito, M., Fukuda, S., Sakata, S., Morinaga, H., & Ohta, T. (2014). Pharmacological effects of JTT-551, a novel protein tyrosine phosphatase 1B inhibitor, in diet-induced obesity mice. *Journal Diabetes Research*, *2014*, 680348.

Jiang, B., Guo, S., Shi, D., Guo, C., & Wang, T. (2013). Discovery of novel bromophenol 3,4-dibromo-5-(2-bromo-3,4-dihydroxy-6-(isobutoxymethyl)benzyl)benzene-1,2-diol as protein tyrosine phosphatase 1B inhibitor and its anti-diabetic properties in C57BL/KsJ-db/db mice. *European Journal of Medicinal Chemistry*, *64*, 129–136. https://doi.org/10.1016/j.ejmech.2013.03.037

Jiang, B., Shi, D., Cui, Y., & Guo, S. (2012). Design, synthesis, and biological evaluation of bromophenol derivatives as protein tyrosine phosphatase 1B inhibitors. *Arch Pharm (Weinheim)*, *345*, 444–453. https://doi.org/10.1002/ardp.201100373

Johnson, T. O., Ermolieff, J., & Jirousek, M. R. (2002). Protein tyrosine phosphatase 1B inhibitors for diabetes. *Nature Reviews Drug Discovery*, *1*, 696–709. https://doi.org/10.1038/nrd895

Kenner, K. A., Anyanwu, E., Olefsky, J. M., & Kusari, J. (1996). Protein-tyrosine phosphatase 1B is a negative regulator of insulin- and insulin-like growth factor-I-stimulated signaling. *The Journal of Biological Chemistry*, *271*, 19810–19816. https://doi.org/10.1074/jbc.271.33.19810

Klaman, L. D., Boss, O., Peroni, O. D., Kim, J. K., Martino, J. L., Zabolotny, J. M., … Kahn, B. B. (2000). Increased energy expenditure, decreased adiposity, and tissue-specific insulin sensitivity in protein-tyrosine phosphatase 1B-deficient mice. *Molecular and Cellular Biology*, *20*, 5479–5489. https://doi.org/10.1128/MCB.20.15.5479-5489.2000

Krishnan, N., Bonham, C. A., Rus, I. A., Shrestha, O. K., Gauss, C. M., Haque, A., … Tonks, N. K. (2018). Harnessing insulin- and leptin-induced oxidation of PTP1B for therapeutic development. *Nature Communications*, *9*, 283. https://doi.org/10.1038/s41467-017-02252-2

Lantz, K. A., Hart, S. G., Planey, S. L., Roitman, M. F., Ruiz-White, I. A., Wolfe, H. R., et al. (2010). Inhibition of PTP1B by trodusquemine (MSI-1436) causes fat-specific weight loss in diet-induced obese mice. *Obesity*, *18*, 1516–1523. https://doi.org/10.1038/oby.2009.444

Leroith, D., & Accili, D. (2008). Mechanisms of disease: Using genetically altered mice to study concepts of type 2 diabetes. *Nature Clinical Practice Endocrinology & Metabolism*, *4*, 164–172. https://doi.org/10.1038/ncpendmet0729

Li, C., Luo, J., Guo, S., Jia, X., Guo, C., Li, X., … Shi, D. (2019). Highly selective protein tyrosine phosphatase inhibitor, 2,2′,3,3′-tetrabromo-4,4′,5,5′-tetrahydroxydiphenylmethane, ameliorates type 2 diabetes mellitus in BKS db mice. *Molecular Pharmaceutics*, *16*, 1839–1850. https://doi.org/10.1021/acs.molpharmaceut.8b01106

Li, K., Li, X. M., Ji, N. Y., & Wang, B. G. (2007). Natural bromophenols from the marine red alga *Polysiphonia urceolata* (Rhodomelaceae): Structural elucidation and DPPH radical-scavenging activity. *Bioorganic & Medicinal Chemistry*, *15*, 6627–6631. https://doi.org/10.1016/j.bmc.2007.08.023

Liao, L. X., Song, X. M., Wang, L. C., Lv, H. N., Chen, J. F., Liu, D., … Tu, P. F. (2017). Highly sselective inhibition of IMPDH2 provides the basis of antineuroinflammation therapy. *Proceedings of the National Academy of Sciences of the United States of America*, *114*, E5986–E5994. https://doi.org/10.1073/pnas.1706778114

Lilley, E., Stanford, S. C., Kendall, D. E., Alexander, S. P., Cirino, G., Docherty, J. R., … Ahluwalia, A. (2020). ARRIVE 2.0 and the British Journal of Pharmacology: Updated guidance for 2020. *British Journal of Pharmacology*. https://bpspubs.onlinelibrary.wiley.com. https://doi.org/10.1111/bph.15178

Liu, S., Xi, Y., Bettaieb, A., Matsuo, K., Matsuo, I., Kulkarni, R. N., & Haj, F. G. (2014). Disruption of protein-tyrosine phosphatase 1B expression in the pancreas affects β-cell function. *Endocrinology*, *155*, 3329–3338. https://doi.org/10.1210/en.2013-2004

Luo, J., Jiang, B., Li, C., Jia, X., & Shi, D. (2019). CYC27 synthetic derivative of bromophenol from red alga *Rhodomela confervoides*: Anti-diabetic effects of sensitizing insulin signaling pathways and modulating RNA splicing-associated RBPs. *Marine drugs*, *17*.

Luo, J., Xu, Q., Jiang, B., Zhang, R., Jia, X., Li, X., … Shi, D. (2018). Selectivity, cell permeability and oral availability studies of novel bromophenol derivative HPN as protein tyrosine phosphatase 1B inhibitor. *British Journal of Pharmacology*, *175*, 140–153. https://doi.org/10.1111/bph.14080

Maedler, K., Carr, R. D., Bosco, D., Zuellig, R. A., Berney, T., & Donath, M. Y. (2005). Sulfonylurea induced β-cell apoptosis in cultured human islets. *The Journal of Clinical Endocrinology and Metabolism*, *90*, 501–506. https://doi.org/10.1210/jc.2004-0699

Malve, H. (2016). Exploring the ocean for new drug developments: Marine pharmacology. *Journal of Pharmacy & Bioallied Sciences*, *8*, 83–91. https://doi.org/10.4103/0975-7406.171700

Martinez Molina, D., Jafari, R., Ignatushchenko, M., Seki, T., Larsson, E. A., Dan, C., et al. (2013). Monitoring drug target engagement in cells and tissues using the cellular thermal shift assay. *Science*, *341*, 84–87. https://doi.org/10.1126/science.1233606

Mikami, D., Kurihara, H., Kim, S. M., & Takahashi, K. (2013). Red algal bromophenols as glucose 6-phosphate dehydrogenase inhibitors. *Marine Drugs*, *11*, 4050–4057. https://doi.org/10.3390/md11104050

Mittermayer, F., Caveney, E., De Oliveira, C., Gourgiotis, L., Puri, M., Tai, L. J., et al. (2015). Addressing unmet medical needs in type 2 diabetes: A narrative review of drugs under development. *Current Diabetes Reviews*, *11*, 17–31. https://doi.org/10.2174/1573399810666141224121927

Mok, A., Cao, H., Zinman, B., Hanley, A. J., Harris, S. B., Kennedy, B. P., et al. (2002). A single nucleotide polymorphism in protein tyrosine phosphatase PTP-1B is associated with protection from diabetes or impaired glucose tolerance in Oji-Cree. *The Journal of Clinical Endocrinology and Metabolism*, *87*, 724–727. https://doi.org/10.1210/jcem.87.2.8253

Mooradian, A. D. (2009). Dyslipidemia in type 2 diabetes mellitus. *Nature Clinical Practice Endocrinology & Metabolism*, *5*, 150–159. https://doi.org/10.1038/ncpendmet1066

Pai, M. Y., Lomenick, B., Hwang, H., Schiestl, R., McBride, W., Loo, J. A., & Huang, J. (2015). Drug affinity responsive target stability (DARTS) for small-molecule target identification. *Methods in Molecular Biology*, *1263*, 287–298. https://doi.org/10.1007/978-1-4939-2269-7_22

Percie du Sert, N., Hurst, V., Ahluwalia, A., Alam, S., Avey, M. T., Baker, M., … Würbel, H. (2020). The ARRIVE guidelines 2.0: Updated guidelines for reporting animal research. *PLoS Biology*, *18*(7), e3000410. https://doi.org/10.1371/journal.pbio.3000410

Schasfoort, R. B. (2017). *Handbook of surface plasmon resonance*. Royal Society of Chemistry. DOI: https://doi.org/10.1039/9781788010283

Shi, D., Xu, F., He, J., Li, J., Fan, X., & Han, L. (2008). Inhibition of bromophenols against PTP1B and anti-hyperglycemic effect of *Rhodomela confervoides* extract in diabetic rats. *Chinese Science Bulletin*, *53*, 2476–2479.

Takahashi, A., Nagashima, K., Hamasaki, A., Kuwamura, N., Kawasaki, Y., Ikeda, H., … Seino, Y. (2007). Sulfonylurea and glinide reduce insulin content, functional expression of K (ATP) channels, and accelerate apoptotic β-cell death in the chronic phase. *Diabetes Research and Clinical Practice*, *77*, 343–350. https://doi.org/10.1016/j.diabres.2006.12.021

Thareja, S., Aggarwal, S., Bhardwaj, T. R., & Kumar, M. (2012). Protein tyrosine phosphatase 1B inhibitors: A molecular level legitimate approach for the management of diabetes mellitus. *Medicinal Research Reviews*, *32*, 459–517. https://doi.org/10.1002/med.20219

Wang, P., Fiaschi-Taesch, N. M., Vasavada, R. C., Scott, D. K., Garcia-Ocana, A., & Stewart, A. F. (2015). Diabetes mellitus—Advances and challenges in human β-cell proliferation. *Nature Reviews. Endocrinology*, *11*, 201–212. https://doi.org/10.1038/nrendo.2015.9

Wu, N., Luo, J., Jiang, B., Wang, L., Wang, S., Wang, C., … Shi, D. (2015). Marine bromophenol bis (2,3-dibromo-4,5-dihydroxy-phenyl)-methane inhibits the proliferation, migration, and invasion of hepatocellular carcinoma cells via modulating β1-integrin/FAK signaling. *Marine Drugs*, *13*, 1010–1025. https://doi.org/10.3390/md13021010

Xiao, P., Wang, X., Wang, H. M., Fu, X. L., Cui, F. A., Yu, X., … Sun, J. P. (2014). The second-sphere residue T263 is important for the function and catalytic activity of PTP1B via interaction with the WPD-loop. *The International Journal of Biochemistry & Cell Biology*, *57*, 84–95. https://doi.org/10.1016/j.biocel.2014.10.004

Zasloff, M., Williams, J. I., Chen, Q., Anderson, M., Maeder, T., Holroyd, K., … McLane, M. (2001). A spermine-coupled cholesterol metabolite from the shark with potent appetite suppressant and antidiabetic properties. *Int J Obesity*, *25*, 689–697. https://doi.org/10.1038/sj.ijo.0801599

Zhang, S., & Zhang, Z. Y. (2007). PTP1B as a drug target: Recent developments in PTP1B inhibitor discovery. *Drug Discovery Today*, *12*, 373–381. https://doi.org/10.1016/j.drudis.2007.03.011

Zhang, Z. Y., Dodd, G. T., & Tiganis, T. (2015). Protein tyrosine phosphatases in hypothalamic insulin and leptin signaling. *Trends in Pharmacological Sciences*, *36*, 661–674. https://doi.org/10.1016/j.tips.2015.07.003

Zheng, Y., Ley, S. H., & Hu, F. B. (2018). Global aetiology and epidemiology of type 2 diabetes mellitus and its complications. *Nature Reviews. Endocrinology*, *14*, 88–98. https://doi.org/10.1038/nrendo.2017.151

## SUPPORTING INFORMATION

Additional supporting information may be found online in the Supporting Information section at the end of this article.

**How to cite this article:** Luo J, Zheng M, Jiang B, et al. Antidiabetic activity in vitro and in vivo of BDB, a selective inhibitor of protein tyrosine phosphatase 1B, from *Rhodomela confervoides*. *Br J Pharmacol*. 2020;177:4464–4480. https://doi.org/10.1111/bph.15195